Astronomy & Astrophysics manuscript no. main
April 7, 2015

Nickel mass estimates of Type Ia Supernovae from Near Infrared data

Suhail Dhawan[1,2,3], B. Leibundgut[1,2], J. Spyromilio[1], and S. Blondin[4]

[1] European Southern Observatory, Karl-Schwarzschild-Strasse 2, D-85748 Garching bei München, Germany
e-mail: sdhawan@eso.org
[2] Excellence Cluster Universe, Technische Universität München, Boltzmannstrasse 2, D-85748, Garching, Germany

[3] Physik Department, Technische Universität München, James-Franck-Strasse 1, D-85748 Garching bei München

[4] Aix Marseille Universit, CNRS, LAM (Laboratoire d'Astrophysique de Marseille) UMR 7326, 13388 Marseille, France

Preprint online version: April 7, 2015

Abstract

Aims. To determine the relation between the total amount of radioactive Nickel (^{56}Ni) produced in Type Ia supernovae (SNIa) and the timing of the second maximum (t_2) in the Near Infrared (NIR; YJH) bands and to extrapolate Nickel mass values for highly reddened SNIa using this relation
Methods. We measure the (pseudo)-bolometric luminosity at peak from the ultraviolet optical Near Infrared (UVOIR) light curves and use it to derive a value for the amount of ^{56}Ni produced ($M_{^{56}Ni}$) for a sample of objects with very little reddening from the host galaxy.Therefore, the effects from presuming a reddening law are smaller.
Results. We find a strong correlation between the peak bolometric luminosity (L_{max}) and t_2 in the Y and J bands and a weaker trend in the H band. We use this empirical relation to derive L_{max} and therefore, $M_{^{56}Ni}$ for test case SNae with high extinction. This allows us to have a $M_{^{56}Ni}$ value which is independent of the reddening law applied. We also apply the relation to all objects not in the low-reddening sample for which a t_2 is measured.
Conclusions. From our results we conclude that an empirical relation between L_{max} and t_2 can allow us to infer the $M_{^{56}Ni}$.The estimates from this method for nearby highly reddened SNae are consistent with independent estimates in the literature. Using the t_2 parameter, we measure the L_{max} for a large sample of SNe and conclude that they have a diverse range of bolometric peaks, and hence a range of $M_{^{56}Ni}$ indicating a significant variation in the explosion mechanism

Key words. supernovae:general - distance scale

1. Introduction

Type Ia supernovae (SNe Ia) exhibit diverse observable properties. In addition to the spectral and colour differences, the peak luminosity of SNe Ia range over several factors (eg. Suntzeff 1996, 2003; Li et al. 2011). The amount of ^{56}Ni derived from the bolometric luminosity (Contardo, Leibundgut & Vacca 2000) and the total ejecta mass (Stritzinger et al. 2006; Scalzo et al. 2014) also show a wide range of values. The $M_{^{56}Ni}$ distribution provides insight into the possible progenitor channels and explosion mechanisms for SNe Ia (see Hillebrandt & Niemeyer 2000; Livio 2000; Truran, Glasner, & Kim 2012).

$M_{^{56}Ni}$ is derived from multi-band ("pseudo-bolometric") light curves using the peak luminosity. Following Arnett (1982) the peak luminosity corresponds to the time when the instantaneous energy input from the decay chain equals the emitted energy. The bolometric light curve is calculated from the magnitudes observed in the different filters. Due to interstellar dust a correction for reddening in the Milky Way and host galaxy needs to be applied. The total to selective absorption (R_V) appears systematically and significantly lower in the SN hosts that the canonical Milky Way (MW) value of 3.1. Nobili & Goobar (2008) use a sample of 80 SNIa with $E(B-V) \leq 0.7$ to derive an average R_V of 1.75 ± 0.27. Although this was revised to more 'normal' values of 2.8 ± 0.3 (Chotard et al. 2011), objects with high extinction (typically $E(B-V)$=0.4 or higher) have an unusually low R_V (Phillips et al. 2013; Scolnic et al. 2014; Patat et al. 2014). The uncertainty in the reddening correction directly impacts the ability to derive accurate bolometric luminosities and hence nickel masses. If a way could be found to derive nickel masses from observables, which are independent of the luminosity, the nickel mass distribution could be determined more accurately.

Near infrared (NIR) observations of SNe Ia provide a promising new approach, which was mostly advocated for improved distance measurements (Meikle 2000; Krisciunas et al. 2007; Wood-Vasey et al. 2008; Barone-Nugent et al. 2012). The uniformity of the NIR peak luminosities together with the reduced effect of absorption yield distances with the uncertainties of light curve fitting and reddening corrections essentially removed. NIR light curves provide interesting clues on the physics of the explosions. In particular the rebrightening of SNe Ia about 2 weeks after the first maximum holds interesting information provide interesting clues on the physics of the explosions. In particular the rebrightening of SNe Ia about 2 weeks after the first maximum holds interesting information on the structure of the explosion (Dhawan et al. 2015). The phase of the second maxi-

Send offprint requests to: TBD

mum shows a strong correclation with the optical decline rate of SNe Ia (Δm_{15}).

Dhawan et al. (2015) found that more luminous SNe Ia reach the second maximum in YJH filters at a later phase as predicted by Kasen (2006). He also predicted that the phase of the second maximum was a function of the iron mass. The phase of the second maximum shows a strong correclation with the optical decline rate of SNe Ia (Δm_{15}). Since the SN Ia luminosity is driven by the amount of $M_{^{56}Ni}$ synthesised in the explosion we conjecture that the phase of the second NIR maximum can be used to measure nickel masses.

In the following, we investigate, directly, the link between the peak bolometric luminosity (L_{max}), and therefore $M_{^{56}Ni}$, and the phase of the second maximum in the NIR light curves (t_2). We use a sample of nearby low-absorption objects (described in section 2) to determine L_{max} and use different methods to derive $M_{^{56}Ni}$ from it (section 2). This relation can then be used to derive $M_{^{56}Ni}$ for all SNe Ia with a measured t_2, since the timing parameter is free of reddening corrections and allows us to include heavily reddened objects, e.g. the nearby SN2014J in M82 (section 4. The phase independent of distance and is not influenced by peculiar velocities of the host galaxies. We discuss the implications of this determination of the $M_{^{56}Ni}$ distribution in the conclusions section 5.

2. Data

The sample for this study is constrained by SNe Ia which have NIR observations at late times as well as well-sampled optical and NIR light curves to construct a (pseudo-)bolometric light curve. The main data source of near-infrared photometry of SNe Ia currently comes from the Carnegie Supernova Project (CSP; Contreras et al. 2010; Burns et al. 2011; Stritzinger et al. 2011; Phillips 2012; Burns et al. 2014). We add to this sample objects from the literature. The full description of the selected SNe Ia can be found in Dhawan et al. (2015).

A sample of SNe Ia with low reddenning is defined to circumvent the uncertainties of host galaxy extinction. Only objects with $E(B-V)_{host} < 0.1$ mag were included (see Table 1). The values for $E(B-V)_{host}$ were taken from the literature references indicated in the Table. Like in Dhawan et al. (2015), we only included objects, which display the second maximum in their NIR light curves. This means that peculiar SNe Ia were excluded.

To construct meaningful bolometric light curves we only included SNe Ia with observations near maximum from u to H filters. No corrections for missing passbands were attempted. These constraints yield a final sample of 18 objects presented in Table 1.

3. Analysis

The integrated flux emitted by an SN Ia in the UV, optical and NIR traces the comptonization of the $\gamma-$rays emitted through the ^{56}Ni $\rightarrow$ ^{56}Co $\rightarrow$ ^{56}Fe decay chain (see Nadyozhin 1994). As the SN emits most of its flux in the UV to NIR passbands, the "UVOIR bolometric flux" represents a physically meaningful quantity (Suntzeff 1996)

We selected a low-reddening sample of objects with a host extinction less than 0.1mag . This makes our measurements less sensitive to the reddening law. We constructed UBVRIJH bolometric light curves for objects with sufficient photometry near maximum light in the optical and the NIR. The K band data was not included since only few SN Ia have well-sampled K band light curves. For a few SN Ia with sufficient K light curves we calculated the fraction of the flux emitted in K and determined it to be around $1-3\%$. Therefore, the exclusion of the K-flux results in only a minor uncertainty.

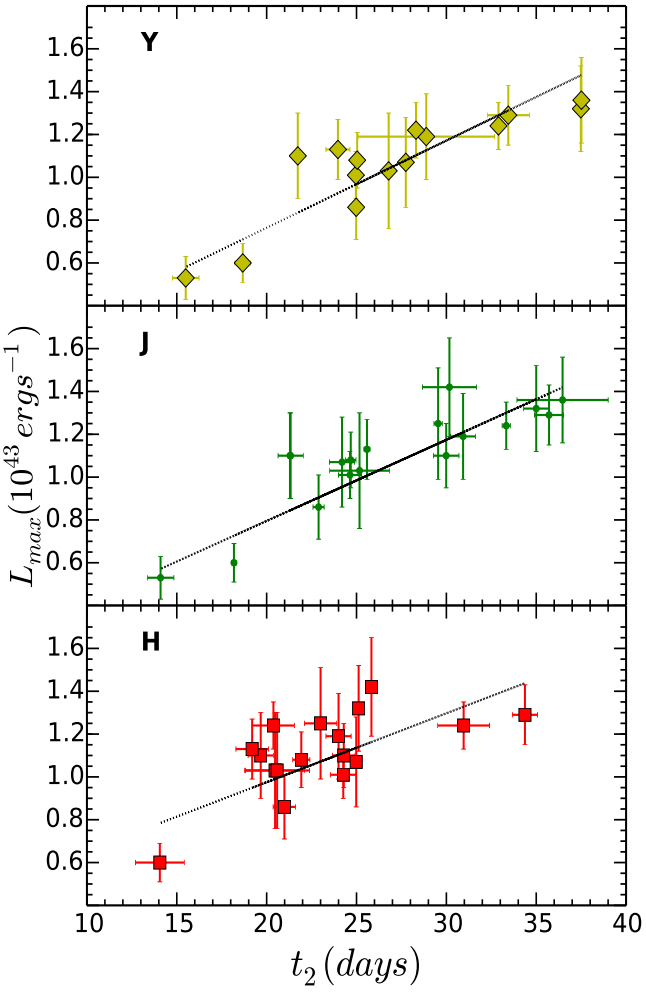

Figure 1. The bolometric maximum luminosity L_{max} is plotted against the phase of the second maximum t_2 in YJH filter light curves. A strong correlation is observed in Y and J, whereas a weaker correlation is seen in the H band. Best fit lines are overplotted in black.

The small reddening correction following CCM was applied to our data before integrating over the available passbands and the uncertainty propagated into the bolometric flux. We use a distance scale of $H_0 = 70\ km\ s^{-1}\ Mpc^{-1}$ and the assumed distances are indicated in Table 3. For the nearby SN Ia with distance measurements provided through direct methods (e.g. Cepheid stars, Tully-Fisher relation) we made sure to employ the same distance scale.

We restricted the analysis to SN Ia with filter coverage from u to H filters and good temporal coverage around the bolometric maximum.

Table 1. The sample of SNe which have low reddening as defined in the text. The references for the SN Ia are presented along with the extinction values and the distances used to calculate the bolometric light curves.

SN	μ	$E(B-V)_{host}$	$E(B-V)_{MW}$	Reference	$t_2(Y)$	$t_2(J)$	$t_2(H)$	$L_{max}(\cdot 10^{43} ergs^{-1})$
SN2002dj	31.70 ± 0.30	0.096 ± 0.030	0.010 ± 0.003	P08	...	31.1 ± 1.8	23.0 ± 0.9	1.25 ± 0.26
SN2002fk	32.59 ± 0.15	0.009 ± 0.044	0.035 ± 0.003	C14	...	29.5 ± 0.2	25.8 ± 0.3	1.42 ± 0.23
SN2005M	35.01 ± 0.09	0.060 ± 0.021	0.027 ± 0.002	B14	28.9 ± 3.8	30.9 ± 0.7	...	1.19 ± 0.20
SN2005am	32.85 ± 0.20	0.053 ± 0.017	0.043 ± 0.002	B14	21.7 ± 0.1	21.3 ± 0.7	19.7 ± 0.7	1.10 ± 0.20
SN2005el	34.04 ± 0.14	0.015 ± 0.012	0.098 ± 0.001	B14	25.0 ± 0.1	24.6 ± 0.6	24.3 ± 0.7	1.01 ± 0.11
SN2005eq	35.46 ± 0.07	0.044 ± 0.024	0.063 ± 0.003	B14	37.5 ± 0.1	35.0 ± 0.7	25.1 ± 0.1	1.32 ± 0.20
SN2005hc	36.50 ± 0.05	0.049 ± 0.019	0.028 ± 0.001	B14	37.5 ± 0.1	36.5 ± 2.5	...	1.36 ± 0.30
SN2005iq	35.80 ± 0.15	0.040 ± 0.015	0.019 ± 0.001	B14	27.7 ± 0.1	24.2 ± 0.7	25.0 ± 0.1	1.07 ± 0.21
SN2005ki	34.73 ± 0.10	0.016 ± 0.013	0.027 ± 0.001	B14	26.8 ± 0.1	25.2 ± 1.7	20.5 ± 1.7	1.03 ± 0.27
SN2006bh	33.28 ± 0.20	0.037 ± 0.013	0.023 ± 0.001	B14	25.0 ± 0.3	22.9 ± 0.3	21.0 ± 0.6	0.86 ± 0.15
SN2007bd	35.73 ± 0.07	0.058 ± 0.022	0.029 ± 0.001	B14	28.3 ± 0.1	...	...	1.22 ± 0.13
SN2007on	31.45 ± 0.08	< 0.007	0.010 ± 0.001	B14	18.7 ± 0.4	18.2 ± 0.1	14.1 ± 1.4	0.60 ± 0.09
SN2008R	33.73 ± 0.16	0.009 ± 0.013	0.062 ± 0.001	B14	15.5 ± 0.7	14.1 ± 0.7	...	0.53 ± 0.10
SN2008bc	34.16 ± 0.13	< 0.019	0.225 ± 0.004	B14	32.9 ± 0.3	33.3 ± 0.2	31.0 ± 1.4	1.24 ± 0.19
SN2008gp	35.79 ± 0.06	0.098 ± 0.022	0.104 ± 0.005	B14	33.5 ± 1.2	35.7 ± 0.8	34.4 ± 0.7	1.29 ± 0.14
SN2008hv	33.84 ± 0.15	0.074 ± 0.023	0.028 ± 0.001	B14	25.0 ± 0.3	24.7 ± 0.3	21.9 ± 0.5	1.08 ± 0.16
SN2008ia	34.96 ± 0.09	0.066 ± 0.016	0.195 ± 0.005	B14	24.0 ± 0.7	25.6 ± 0.2	19.2 ± 0.9	1.13 ± 0.14
SN2011fe	28.91 ± 0.20	0.014 ± 0.010	0.021 ± 0.001	P13	...	30.0 ± 0.8	24.3 ± 0.6	1.10 ± 0.15

E(B-V) references: P08: Pignata et al. (2008); C14: Cartier et al. (2014) B14:Burns et al. (2014); P13: Patat et al. (2013)

4. Results

Using a sample of SN Ia with known small absorption we correlate the bolometric peak luminosity with light curve parameters. This should allow us to investigate whether the nickel mass can be determined from distance independent parameters. If there exist a relation between the light curve characteristics and the nickel mass, in particular the phase of the second maximum in the near-infrared light curves that only weakly depends on absorption, we can then apply them to a larger sample with unkown host galaxy absorption.

4.1. Low galactic reddening sample

We selected objects with a host galaxy extinction of $E(B-V) < 0.1$. For some of these objects the total Milky Way and host galaxy extinction is $E(B-V))_{tot} > 0.1$. Although the Milky Way extinction law is well established, we investigated whether these objects influence the strength of the correlation. As a result, 7 objects with $E(B-V)_{host} < 0.1$ but total $E(B-V) \geq 0.1$ were removed in this low galactic reddening sample. The slopes and intercepts derived for this subsample of 10 objects are within error bars of the values in Table 2 for all 3 filters. Interestingly, several of these objects are amongst the most luminous objects in the sample. In particular in H all luminous objects are removed, when we apply this cut and the slope significantly increases due to a single low-luminosity object. This could mean that the luminous objects were over corrected for absorption, however in Y and J the slopes increase only very slightly and well within the respective uncertainties.

4.2. Correlation between L_{max} and t_2

Dhawan et al. (2015) found a strong correlation between the phase of the second maximum in the near-infrared light curves (t_2) and various indicators of the optical luminosity of SNe Ia. In particular the optical light curve shape parameter Δm_{15} correlates strongly with t_2 in the Y and J filters. Additional correlations were found with the onset of the Lira law in the $(B-V)$ colour and the NIR luminosity at late ($t > 55$days) phases. It was surmised that all these parameters are directly linked to the nickel mass in the explosion (see Dhawan et al. 2015, for details).

Table 2. Values of the coefficients for correlations between L_{max} and t_2 in the individual filters

Filter	a_i	b_i
Y	0.041 ± 0.005	-0.065 ± 0.122
J	0.039 ± 0.004	0.013 ± 0.106
H	0.032 ± 0.008	0.282 ± 0.174

Figure 1 displays a very strong correlation between t_2 for the Y and J filter light curves and the bolometric (UVOIR) luminosity L_{max} with Pearson correlations $r = 0.88$ and $r = 0.86$, respectively, in the low-reddening sample defined in Section 2 and Table 1. A much weaker trend is observed in the H filter light curve with $r \approx 0.60$.

In the Y and J band, a strong correlation suggests that more luminous objects show later second maxima.

$$L_{max} = a_i \cdot t_{2,i} + b_i \quad (1)$$

From Table 2 and Figure 1, we can see that the constraints on the slope for the best fit relation in the H band are weak. The distribution of $t_{2,H}$ appears more clumped than in the other filters and one extreme object (SN 2008R with the lowest luminosity) has no second maximum measured in H. It will have to be seen, whether future data will reveal a correlation or whether the H light curves are not as sensitive to the nickel mass (see below) as the other NIR filters. The relations for t_2 in Y and J vs. the bolometric peak luminosity $L_{max}$are very similar. Table 2 shows that the slope values for the two bands are nearly identical and the intercepts are within the error. We combine the relations from the two bands for extrapolating the values of L_{max} in the following analysis. We assume the Y band estimate to be equivalent to the

value in the J band and calculate the slope and intercept with the photometry of both filters, which leads to a reduction in the errors on the parameter estimates.

4.3. Deriving $M_{^{56}Ni}$ from L_{max}

Our final goal is to use t_2 to derive a value of the $M_{^{56}Ni}$. Hence, we present the different methods to derive $M_{^{56}Ni}$ from L_{max}. In this section we detail 3 methods to derive $M_{^{56}Ni}$ from L_{max}, namely, using Arnett's rule with a rise time specific to the SN, using Arnett's rule with a fixed rise time applied to all SN, and by interpolating the values for L_{max} and $M_{^{56}Ni}$ from delayed detonation models (Blondin et al. 2013).

4.3.1. Arnett's rule with a variable rise time

Arnett's rule states that the luminosity of the SN at peak is given by the instantaneous rate of energy deposition from radioactive decays inside the expanding ejecta (Arnett 1982; Arnett et al. 1985).

This is summarized in equation (2)

$$L_{max}(t_R) = \alpha E_{Ni}(t_R). \quad (2)$$

Where E_{Ni} is the input from ^{56}Ni and ^{56}Co decays at maximum, t_R is the rise time and α accounts for deviations from Arnett's Rule. The energy output from 1 solar mass of nickel is then:

$$\epsilon_{Ni}(t_R, 1\,M_\odot) = (6.45{\cdot}10^{43}e^{-t_R/8.8}{+}1.45{\cdot}10^{43}e^{-t_R/111.3})\mathrm{erg/s} \quad (3)$$

For estimates using different rise times in the B filter for each SN, we use the following relation

$$t_{R,B} = 17.5 - 5(\Delta m_{15} - 1.1) \quad (4)$$

from Scalzo et al. (2014) which covers the $t_{R,B}$–Δm_{15} parameter space of Ganeshalingam, Li, & Filippenko (2011). As in Scalzo et al. (2014), we apply a conservative uncertainty estimate of ± 2 days.

The bolometric rise occurs on average 1 day before the B_{max}, hence Equation (3) now reads

$$L_{max}(t_{R,bol}) = \alpha \cdot [\epsilon_{ni}(t_R, M_\odot) \cdot (M_{^{56}Ni}/M_\odot)]\mathrm{erg/s} \quad (5)$$

substituting the relation derived between L_{max} and t_2 (equation (1)) we obtain a relation between t_2 and $M_{^{56}Ni}$

$$\frac{M_{^{56}Ni}}{M_\odot} = \frac{a_i \cdot t_2(i) + b_i}{\alpha \cdot \epsilon_{Ni}(t_{R,bol}, M_\odot)}. \quad (6)$$

4.3.2. Arnett's rule with a fixed rise time

For this method of deriving $M_{^{56}Ni}$ from L_{max}, we use a fixed rise time of 19 days, for all SNe, as in Stritzinger et al. (2006). Similar to their analysis, we propagate an uncertainty of $\pm$ 3 days, to account for the diversity in the rise times. The peak luminosity then becomes (Stritzinger et al. 2006)

$$L_{max} = (2.0 \pm 0.3) \cdot 10^{43}(M_{^{56}Ni}/M_\odot)\mathrm{erg/s}. \quad (7)$$

This assumes $\alpha = 1$ (see Stritzinger et al. 2006; Mazzali et al. 2007), which is close to the self-consistent models of Arnett (1982) and the mean of several models investigated by Höflich, Khokhlov & Wheeler (1995). Table 1 of Branch (1992) shows the different α values for the numerical light curve calculations to be centered about 1.

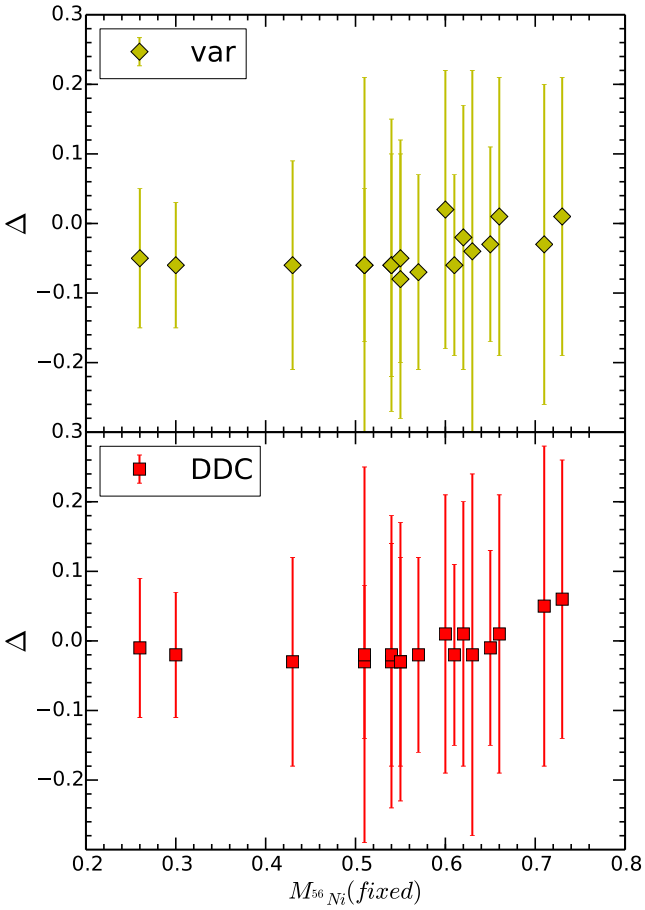

Figure 2. *Top*: The difference between the values estimated using a fixed rise time with Arnett's rule and the DDC models is plotted against the estimates from Arnett's rule with fixed rise time. *Bottom*: The difference between values estimated using a fixed rise time with Arnett's rule and a variable rise time plotted against the estimates from Arnett's rule with fixed rise time. From the two panels we can see that the difference in the individual measurements are much smaller than the errors on the measured values.

4.3.3. Interpolating using DDC models

We use the DDC models from Blondin et al. (2013) as another method of obtaining $M_{^{56}Ni}$ from the peak luminosity. The luminosity can be calculated from the models and the time of equality of energy input and instantaneous release at the surface determined from the radiation transport. This yields an independent route to the value of α. The output value of α from the DDC models ranges from 0.94 to 1.18 with a mean value of 1.04. Hence, we find that the output α value is consistent with the $\alpha = 1$ to within 18%.

For objects without NIR coverage the models can be used to calculate the $M_{^{56}Ni}$–L_{max} relationship for a set of optical-only filters. This allows us to include objects, which do not have the full wavelength coverage to calculate the full bolometric light curves (e.g. SN2004gu only has $BVRI$ coverage near maximum). In principle we can infer the $M_{^{56}Ni}$ values for objects with missing passbands, however, in order to keep the samples uniform across the different methods, we only use the objects with complete coverage from u to H bands.

Table 3. L_{max} measurements for low reddening SNIa with a measured t_2.

SN	$M_{Ni} - Arn(M_\odot)$	$M_{Ni} - Arn(M_\odot)$ (fixed rise)	$M_{Ni} - DDC(M_\odot)$
SN2002dj	0.59 ± 0.18	0.63 ± 0.20	0.61 ± 0.14
SN2002fk	0.68 ± 0.19	0.71 ± 0.20	0.76 ± 0.13
SN2005M	0.62 ± 0.16	0.60 ± 0.18	0.61 ± 0.11
SN2005am	0.47 ± 0.16	0.55 ± 0.15	0.52 ± 0.11
SN2005el	0.45 ± 0.11	0.51 ± 0.11	0.48 ± 0.07
SN2005eq	0.67 ± 0.16	0.66 ± 0.19	0.67 ± 0.11
SN2005hc	0.69 ± 0.20	0.68 ± 0.24	0.71 ± 0.16
SN2005iq	0.48 ± 0.14	0.54 ± 0.16	0.51 ± 0.10
SN2005ki	0.45 ± 0.17	0.51 ± 0.18	0.49 ± 0.14
SN2006bh	0.37 ± 0.11	0.43 ± 0.11	0.40 ± 0.07
SN2007bd	0.55 ± 0.14	0.61 ± 0.17	0.59 ± 0.10
SN2007on	0.24 ± 0.07	0.30 ± 0.07	0.28 ± 0.05
SN2008R	0.21 ± 0.08	0.26 ± 0.07	0.25 ± 0.06
SN2008bc	0.60 ± 0.12	0.62 ± 0.15	0.63 ± 0.11
SN2008gp	0.62 ± 0.15	0.65 ± 0.17	0.64 ± 0.09
SN2008hv	0.48 ± 0.12	0.54 ± 0.15	0.52 ± 0.09
SN2008ia	0.50 ± 0.12	0.57 ± 0.13	0.55 ± 0.09
SN2011fe	0.50 ± 0.12	0.55 ± 0.14	0.52 ± 0.10

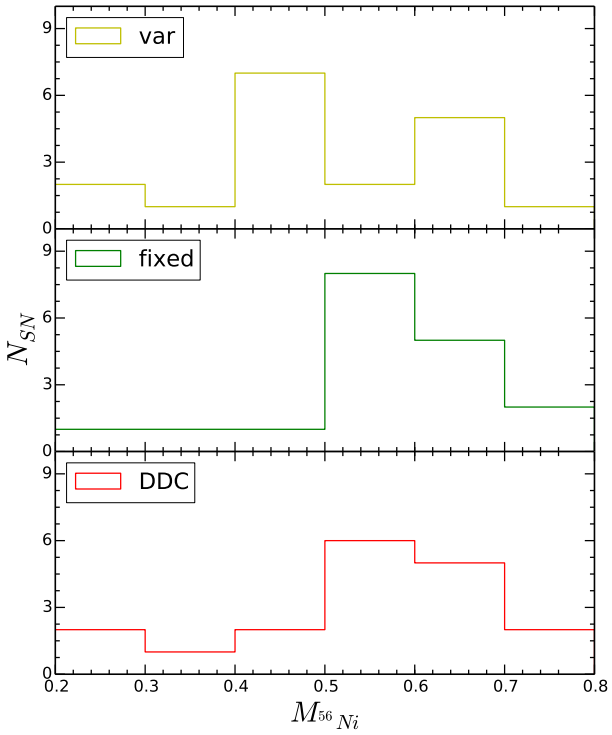

Figure 3. The histograms show the different methods to estimate the $M_{^{56}Ni}$ from the L_{max}. The values from Arnett's rule with fixed and variable rise time are plotted in the *top* and *middle* panels. The *bottom* panel has the values estimated from the DDC models

In Figure 3, we plot the distributions of the $M_{^{56}Ni}$ from the different methods.

Similar to previous studies we find that there is a large distribution in the $M_{^{56}Ni}$ values for the sample in Table 1. We note a factor of $\sim$3 difference between the lowest and highest $M_{^{56}Ni}$ values. Unlike previous studies, this sample doesn't include faint, 91bg-like objects, since their NIR light curves do not display a second maximum. These objects are seen to have a much lower $M_{^{56}Ni}\sim$0.1 $M_\odot$. Thus, the complete distribution of $M_{^{56}Ni}$ for SNIa is expected to be wider than is seen in our sample.

4.4. Test Case for heavily reddened SNe

Dust in the host galaxy and the Milky Way scatters the light from the supernovae. In some cases the extinction is very high ($E(B-V)$ $\sim$1 mag). Large samples of nearby SNe have shown marked deviations in dust properties of SN hosts from those of the Milky Way, with SN hosts favouring a smaller R_V value (Goobar 2008; Phillips et al. 2013). The corrections for extinction are notoriously uncertain and have direct effect on our ability to measure peak bolometric luminosities of SNe Ia. Since t_2 is a reddening independent measurement, we can use the derived correlation to estimate the ^{56}Ni masses for heavily reddened SNe. As a test, we apply this relation to SN2014J, which has a direct $\gamma-$ray detection from the nickel-cobalt decay chain (Churazov et al. 2014; Diehl et al. 2014b).

For this SN, using the bolometric luminosity and Arnett's rule provides values of $M_{^{56}Ni}$ that are heavily dependent on the assumed absorption law for the host galaxy dust, A_V. here is a variation of a factor of $\sim$2 in $M_{^{56}Ni}$ depending on the A_V value used (0.37 $M_\odot$ using A_V=1.7 mag from Margutti et al. (2014), compared to 0.77 using a higher A_V of 2.5 mag from Goobar et al. (2014a).

Using the best fit relation for the reddening-free sample defined in the previous section, we obtain $M_{^{56}Ni} = (0.64 \pm 0.15) M_\odot$ for a $t_2 = (31.99 \pm 1.15)$ days. To obtain this $M_{^{56}Ni}$ from the estimated bolometric peak, we use Arnett's rule with a fixed rise. Since the error on the rise time is taken as $\pm$ 3 days, we expect the error on $M_{^{56}Ni}$ to decrease with a less conservative error estimate on t_R.

This can be compared to the direct measurement of $M_{^{56}Ni}$ for SN2014J through the $\gamma-$ray detection. The proximity of SN2014J, led to the first $\gamma-$ray Co line detection in a SN Ia (Churazov et al. 2014). Using a line photon escape fraction from the models, Churazov et al. (2014) derive $^{56}Ni = 0.62 \pm 0.13 M_\odot$. This method only works for the closest SNe I and more distant objects need a different method.

A detailed comparison of the derived nickel masses is given in Table 4.4. The difficulty of the extinction correction and the

advantage of the method presented here are obvious. The uncertainty in the $\gamma-$ray determination is due to the weakness of the signal and hence slightly different interpretations. Nevertheless, it appears that a consistent mass within a 10% uncertainty has been determined.

The very good correspondence between the direct M_{Ni} measurement and our relation of the second maximum in the NIR light curves is encouraging. It adds evidence to the argument that the NIR can be used for estimating $M_{^{56}Ni}$ for highly reddened SNe.

As a second case, we determine the bolometric peak luminosity L_{max} and the nickel mass $M_{^{56}Ni}$ through t_2 to the heavily extinguished SN 2006X. The second maximum $t_{2,H}$ for SN 2006X occured at (28.19 ± 0.49) days after B maximum. The derived nickel mass is $M_{^{56}Ni} = (0.56 \pm 0.13) M_{\odot}$ and $M_{^{56}Ni} = (0.57 \pm 0.14) M_{\odot}$ for the Y light curve. These values are consistent with the conclusion that SN 2006X is a 'normal' SNIa (Wang et al. 2008).

Wang et al. (2008) measure $M_{^{56}Ni}$ using the bolometric peak luminosity and Arnett's rule. They employed multi-band photometry to correct for absorption from host galaxy dust and derive a bolometric peak luminosity of $(1.02 \pm 0.1) \cdot 10^{43}\ ergs^{-1}$. The R-band rise time to B maximum is $(18.2 \pm 0.9$ days, which leads to $M_{^{56}Ni} = (0.50 \pm 0.05) M_{\odot}$. All determined nickel masses for SN 2006X are consistent with each other.

Three more highly reddened SNe Ia, SN 1986G, SN 2005A and SN 2008fp (Phillips et al. 2013; Patat et al. 2014) were added to the sample. The $M_{^{56}Ni}$ for these objects were calculated in the same way as for SN 2014J and SN 2006X and are summarised in Table 5. For the five objects in Table 5 we used the J-band relation to obtain an $M_{^{56}Ni}$. We also used a combined fit to the Y and J band data to evaluate the reduction in the error bar.

From table 5, we can see that 1986G has a lower value of $M_{^{56}Ni}$ than the other heavily reddened objects. This is consistent with the observed optical decline rate and lower B band luminosity of the SN (Phillips et al. 1987). Using nebular spectra, Ruiz-Lapuente & Lucy (1992) calculate the $M_{^{56}Ni}$for SN1986G and find a value of $0.38 \pm 0.03\ M_{\odot}$. This is fully consistent with the estimate from t_2. There are no nickel masses reported for these supernovae **is this correct?**.

4.4.1. Measured Rise Time

The error in the expression from Arnett's rule relating the L_{max} and $M_{^{56}Ni}$ (equation (7)) arises from our adopted uncertainty of 3 days (using the fixed rise time formalism as in Stritzinger et al. (2006)). However, for objects with early time observations and constraints on time of first light, the error on the rise time is $\sim$1 day.

Goobar et al. (2014b) used Palomar Transient Factory (PTF) and Kilodegree Extremely Little Telescope (KELT) data to measure the rise time of SN 2014J. They find $t_R = 17.25$ days. We place a conservative error estimate of 1 day and evaluate the $M_{^{56}Ni} = (0.62 \pm 0.10) M_{\odot}$ which is an improvement on the fixed rise time formalism.

Similarly, a measured rise time for SN 2006X ($t_{R,B} = (18.2 \pm 0.9)$ days) from Wang et al. (2008) gives an $M_{^{56}Ni} = (0.53 \pm 0.08) M_{\odot}$.

4.5. Complete NIR Sample

We are now in a position to derive L_{max} for all SNe Ia with a reliably measured t_2. Since the phase of the second maximum in the near infrared is independent from the reddening can we derive the reddening-free distribution of the luminosity function of SNe Ia (Fig. 4). We show here the histograms of the true bolometric peak luminosity as derived from the Y and J light curves. **Since we combined the analysis before, we should do this here as well and only show one histogram.** No corrections for absorption are required.

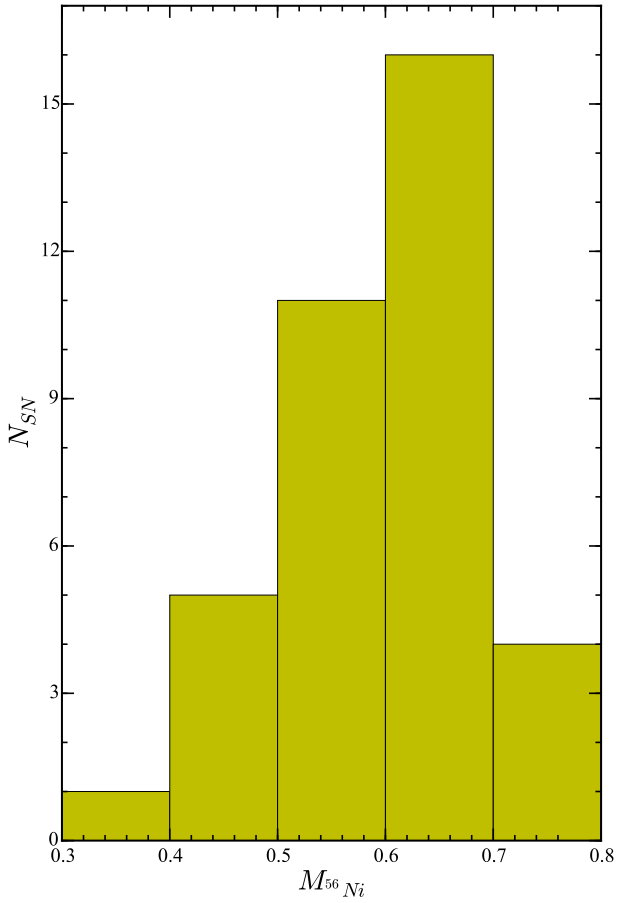

Figure 4. Histogram distribution of $M_{^{56}Ni}$derived from the relations for the complete sample of objects (without the low reddening sample). We use the combined fit to obtain the final values. We derive the $M_{^{56}Ni}$from L_{max} using Arnett's rule with a fixed rise time

The next step is to derive the distribution of $M_{^{56}Ni}$ for all SNe Ia with sufficient infrared light curve data. Table 4.5 and Fig. **??** present the SN Ia nickel mass function.

4.6. Comparison with published values

We searched the literature for published values of $M_{^{56}Ni}$ for objects in our sample. Scalzo et al. (2014) published values of $M_{^{56}Ni}$ for SN 2005el and SN 2011fe. The comparison for SN 2011fe shows $M_{^{56}Ni} = (0.52 \pm 0.15) M_{\odot}$ from the NIR light curves, whereas Scalzo et al. (2014) find $M_{^{56}Ni} = (0.42 \pm 0.08) M_{\odot}$. The difference is mostly in the adopted value of α, which is 20% larger in Scalzo et al. (2014) than used here. Adopting $\alpha = 1.2$ we derive $M_{^{56}Ni} = 0.44 M_{\odot}$ fully consistent with Scalzo et al. (2014). **it would be better to calculate the Scalzo mass for $\alpha = 1$ to have a consistent picture here.** Pereira et al. (2013) report nickel masses for SN 2011fe

Table 4. Comparison of different methods to estimate $M_{^{56}Ni}$ for SN2014J

M_{Ni} (inferred)	σ	Method	Reference
0.62	0.13	γ ray lines	Churazov et al. (2014)
0.50	0.10	γ ray lines	Diehl et al. (2014b)
0.37	–	Bolometric light curve A_V=1.7 mag	Churazov et al. (2014); Margutti et al. (2014)
0.77	–	Bolometric light curve A_V=2.5 mag	Churazov et al. (2014); Goobar et al. (2014a)
0.64	0.13	NIR second maximum	this work (combined fit)
0.62	0.10	NIR second maximum + measured rise	this work

Table 5. M_{Ni} estimates for 5 objects with high values of $E(B-V)_{host}$. We present constraints from the relation using only $t_2(J)$ as well as from both $t_2(Y)$ and $t_2(J)$. We can see a marked decrease in the error values when combined constraints are used

SN	$t_2(J)$	$M_{^{56}Ni}$ (inferred)	σ	μ	A_V[a] (mag)	Method
SN1986G	16.40 ± 1.4	0.34	0.10	28.01 ± 0.12	2.03	J band relation
–	–	0.35	0.08	–	–	combined fit
SN2005A	27.58 ± 0.3	0.56	0.13	34.51 ± 0.11	1.58	J band relation
–	–	0.56	0.11	–	–	combined fit
SN2006X	28.19 ± 0.5	0.56	0.13	30.91 ± 0.08	1.88	J band relation
–	–	0.57	0.11	–	–	combined fit
SN2008fp	31.03 ± 0.3	0.62	0.15	31.79 ± 0.05	0.71	J band relation
– -	–	0.62	0.13	–	–	combined fit
SN2014J	31.99 ± 1.2	0.64	0.15	27.64 ± 0.10	1.85	J band relation
–	–	0.64	0.13	–	–	combined fit

[a] References for A_V values: SN1986G, SN2006X, SN2008fp Phillips et al. (2013), SN2005A Burns et al. (2014), SN2014J Amanullah et al. (2014)

for different values of α. Their nickel mass for α=1 is $M_{^{56}Ni} = (0.53 \pm 0.11) M_{\odot}$, nearly identical to our determination.

The only other determination we could find was for SN 2005el. The comparison with the value dervied by Scalzo et al. (2014) ($M_{^{56}Ni} = (0.52 \pm 0.12) M_{\odot}$) and ours ($M_{^{56}Ni} = (0.51 \pm 0.12) M_{\odot}$ is less than 2% and well below the uncertainty. **SN 1999ac is also in Stritzinger et al. 2006 - we need to check this better**.

5. Discussion and Conclusion

The light curves of SN Ia are powered by the ^{56}Ni $\rightarrow$ ^{56}Co $\rightarrow$ ^{56}Fe decay chain (Colgate & McKee 1969). The emerging (bolometric) energy flux at maximum luminosity equals the instantaneous ^{56}Ni decay rate (Arnett 1982). An estimate of the peak bolometric flux provides a direct measurement of the energy source and in particular the $M_{^{56}Ni}$in SNe Ia. This is possibly the most important parameter shaping the appearance of SNe Ia.

Dhawan et al. (2015) showed that the phase of the second maximum t_2 in the Y, J and H light curves tightly correlates with light curve parameters at other wavelengths and is a strong indicator of the amount of iron in a SN Ia. We tested here whether t_2 also correlates with the peak luminosity L_{max}. If so, the NIR light curves would open a reddening free measurment of the maximum energy output and hence the nickel mass $M_{^{56}Ni}$.

We selected a sample of SNe Ia with late time NIR observations and low absorption from host galaxy dust. For these objects L_{max} indeed strongly correlates with t_2 in the Y and J. Different methods to calculate the mass of ^{56}Ni from the L_{max} were discussed. The different method show small differences, which indicates that currently the scatter is dominated mostly by the uncertainty in the data.

Using the relation derived from the low-reddening sample, we extrapolate an L_{max} value for all SNe Ia objects having a measured t_2. The estimate of t_2, along with this relation, provides a method to deduce the bolometric peak luminosity, independent of a reddening estimate, distance measurement (relative to the calibration of our low-absorption sample) and without requiring multi-band photometry. We hence have established a reddening-free luminosity function of SNe Ia at peak.

The nearby SN 2014J in M82, which is heavily reddened by host galaxy dust, was used as a test case. The reddening from the host galaxy introduces a large uncertainty in the measurement of $M_{^{56}Ni}$ from the bolometric light curves (**?**Margutti et al. 2014). Using the t_2 estimate for SN 2014J we obtained an estimate of L_{max} and from it a value for $M_{^{56}Ni}$ which is fully consistent with the direct measurement through the $gamma-$rays from the radioactive decays (Churazov et al. 2014; Diehl et al. 2014b).

We established an instrinsic luminosity function and nickel mass distribution for all SNe Ia with a t_2 measurement 1. We emphasize that this luminosity function is independent of the reddening from host galaxy dust and the distance measurement to the host (relative to the distribution of our calibrator sample). The distribution of L_{max}has a large variance. Since faint 91bg-like SNE Ia do not display a second maximum in their NIR light curve we did not include them in our sample. They show typically luminosities lower than what we have determined here (e.g. Scalzo et al. 2014). **do we have an example for the super-Chandras excluded? "or peculiar super-Chandra explosions,"** The 'true' dispersion is likely to be larger than derived here. For e.g., in Stritzinger et al. (2006) the authors find a dispersion of a factor of $\sim$ 10, since their sample included peculiar SNe Ia like SN 1991bg and SN 1991T.

This large range of L_{max}, and hence, $M_{^{56}Ni}$ estimated from t_2, presents a challenge to the notion that all SN Ia are a result of nuclear burning near the Chandrasekhar mass limit and lends

Table 6. $M_{^{56}Ni}$measurements for the complete sample of objects with t_2 measurements in both Y and J bands.

SN	$M^a_{^{56}Ni}$ (J)	σ^a	$M^a_{^{56}Ni}$ (Y)	σ^a
1980N	0.47	0.10	...	...
1981B	0.68	0.13	...	...
1998bu	0.63	0.12	...	...
1999ac	0.57	0.12	...	...
1999ee	0.73	0.15	...	...
2000E	0.67	0.14	...	...
2000bh	0.70	0.14	...	...
2001bt	0.60	0.12	...	...
2001cn	0.63	0.13	...	...
2001cz	0.69	0.14	...	...
2001el	0.63	0.15	...	...
2002bo	0.57	0.11	...	...
2003cg	0.64	0.13	...	...
2003hv	0.47	0.10	...	...
2004ey	0.62	0.14	0.67	0.15
2004gs	0.48	0.11	0.47	0.11
2004gu	0.75	0.17	0.79	0.17
2005al	0.54	0.13	0.53	0.13
2005na	0.69	0.15	0.58	0.13
2006D	0.54	0.13	0.52	0.13
2006ax	0.68	0.15	0.69	0.16
2006et	0.68	0.16	0.69	0.15
2006gt	0.43	0.09	...	...
2006hb	0.41	0.11	0.37	0.10
2006kf	0.52	0.12	0.55	0.10
2007S	0.75	0.16	0.78	0.17
2007af	0.62	0.14	0.63	0.14
2007as	0.52	0.14	0.48	0.12
2007bm	0.59	0.13	0.68	0.15
2007le	0.65	0.15	0.67	0.15
2007nq	0.50	0.13	0.48	0.12
2008C	0.68	0.16	0.63	0.14

^{a}:$M_\odot$

credibility to the idea that SNIa arise from more than one progenitor channel. There is mounting evidence from ejecta mass reconstructions (Stritzinger et al. 2006; Scalzo et al. 2014) that most SNe produce $<$1.4 $M_\odot$ of ejecta and hence would be better described by sub-Chandrasekhar mass explosions.

Recent, interesting, observations of ^{56}Ni lines at 158 and 812 keV only $\sim$ 20 days post explosion (in SN2014J) indicate the presence of ^{56}Ni on the outskirts of the SN (Diehl et al. 2014a). The authors suggest that this ^{56}Ni could be a result of a mass accretion from an He donor star in a sub-Chandrasekhar mass model. Theoretical efforts have also postulated the presence of ^{56}Ni at shallow depths ($\sim 10^{-2} M_\odot$) in the ejecta (e.g. Piro & Nakar 2013, 2014), which affect the shape of the rising light curves and can explain the deviation of the early light curve of SN 2014J from the t^2 power law rise. However, the ^{56}Ni on the outside would be γ transparent and only contribute a very small fraction to the total bolometric flux near maximum light. Since the ^{56}Ni on the outside is of order 0.05 $M_\odot$ (Diehl et al. 2014a), this is not a very significant contribution to the bolometric peak luminosity. Thus, our measurement of the bolometric peak doesn't offer an estimate of the ^{56}Ni on the outside and hence underestimates the total $M_{^{56}Ni}$.

Studies like Churazov et al. (2015) have explored this possibility using Monte Carlo simulations. They compare the ring model posited in Diehl et al. (2014a) to a spherical shell like distribution of ^{56}Ni. They find that for the spherical shell model the early rise can be explained with only 0.01 $M_\odot$ of ^{56}Ni. In either scenario, the ^{56}Ni on the outside is at least an order of magnitude smaller than the ^{56}Ni embedded deep in the ejecta. Hence, the error from not being sensitive to the ^{56}Ni on the outskirts is very small. The dominant error sources are still from the distance and reddening uncertainties.

Acknowledgements. This research was supported by the DFG cluster of excellence Origin and Structure of the Universe' B.L. acknowledges support for this work by the Deutsche Forschungsgemeinschaft through TRR33, The Dark Universe. We would like to thank Rahman Amanullah for providing published photometry of SN2014J in the near infrared.

References

Amanullah R., et al., 2014, ApJ, 788, 21
Arnett W. D., 1982, ApJ, 253, 785
Arnett W. D., Branch, D., Wheeler, J. C., 1985, Nature, 314, 337
Barone-Nugent R. L., et al., 2012, MNRAS, 425, 1007
Biscardi I., et al., 2012, A&A, 537, A57
Blondin S., Dessart L., Hillier D. J., Khokhlov A. M., 2013, MNRAS, 429, 2127
Blondin S., Dessart L., Hillier D. J., 2015, arXiv, arXiv:1501.06583
Branch D., 1992, ApJ, 392, 35
Burns C. R., et al., 2011, AJ, 141, 19
Burns C. R., et al., 2014, ApJ, 789, 32
Cardelli J. A., Clayton G. C., Mathis J. S., 1989, ApJ, 345, 245
Cartier R., et al., 2014, ApJ, 789, 89
Chotard N., et al., 2011, A&A, 529, L4
Churazov E., et al., 2014, Natur, 512, 406
Churazov E., et al., 2015, arXiv, arXiv:1502.00255
Colgate S. A., McKee C., 1969, ApJ, 157, 623
Contardo G., Leibundgut B., Vacca W. D., 2000, A&A, 359, 876
Contreras C., et al., 2010, AJ, 139, 519
Dhawan S., Leibundgut B., Spyromilio J., Maguire K., 2015, MNRAS, 448, 1345
Diehl R., et al., 2014a, arXiv, arXiv:1407.3061
Diehl R., et al., 2014b, arXiv, arXiv:1409.5477
Filippenko A. V., et al., 1992, AJ, 104, 1543
Firth R. E., et al., 2015, MNRAS, 446, 3895
Foley R., et al., 2014, arXiv, arXiv:1405.3677
Foreman-Mackey D., Hogg D. W., Lang D., Goodman J., 2013, PASP, 125, 306
Ganeshalingam M., Li W., Filippenko A. V., 2011, MNRAS, 416, 2607
Goobar A., 2008, ApJ, 686, L103
Goobar A., et al., 2014, ApJ, 784, L12
Goobar A., et al., 2014, arXiv, arXiv:1410.1363
Goodman J., Weare J., 2010, Comm. App. Math. Comp. Sci. 5 (1), 65.
Hillebrandt W., Niemeyer J. C., 2000, ARA&A, 38, 191
Höflich P., Khokhlov A., Wheeler C., 1995, ASPC, 73, 441
Jensen J. B., Tonry J. L., Barris B. J., Thompson R. I., Liu M. C., Rieke M. J., Ajhar E. A., Blakeslee J. P., 2003, ApJ, 583, 712
Kasen D., 2006, ApJ, 649, 939
Kasen D., Woosley S. E., 2007, ApJ, 656, 661
Kattner S., et al., 2012, PASP, 124, 114
Kelly B. C., 2007, ApJ, 665, 1489
Krisciunas K., Phillips M.M., Suntzeff, N.B., 2004, ApJ, 602, 81
Krisciunas K., et al., 2007, AJ, 133, 58
Leaman J., Li W., Chornock R., Filippenko A. V., 2011, MNRAS, 412, 1419
Leibundgut B., 2000, A&ARv, 10, 179
Leibundgut B., et al., 1993, AJ, 105, 301
Li W., et al., 2011, MNRAS, 412, 1441
Livio M., 2000, tias.conf, 33
Margutti R., Parrent J., Kamble A., Soderberg A. M., Foley R. J., Milisavljevic D., Drout M. R., Kirshner R., 2014, ApJ, 790, 52
Mazzali P. A., Röpke F. K., Benetti S., Hillebrandt W., 2007, Sci, 315, 825
Matheson T., et al., 2012, ApJ, 754, 19
Meikle W. P. S., 2000, MNRAS, 314, 782
Nadyozhin D. K., 1994, ApJS, 92, 527
Nobili S., Goobar A., 2008, A&A, 487, 19
Pakmor R., Kromer M., Taubenberger S., Sim S. A., Röpke F. K., Hillebrandt W., 2012, ApJ, 747, L10
Patat F., et al., 2013, A&A, 549, A62
Patat F., et al., 2014, arXiv, arXiv:1407.0136
Pereira R., et al., 2013, A&A, 554, A27
Phillips M. M., 1993, ApJ, 413, L105
Phillips M. M., 2012, PASA, 29, 434
Phillips M. M., et al., 1987, PASP, 99, 592

Phillips M. M., Lira P., Suntzeff N. B., Schommer R. A., Hamuy M., Maza J., 1999, AJ, 118, 1766
Phillips M. M., et al., 2013, ApJ, 779, 38
Pignata G., et al., 2008, MNRAS, 388, 971
Piro A. L., Nakar E., 2013, ApJ, 769, 6
Piro A. L., Nakar E., 2014, ApJ, 784, 85
Ruiter A. J., et al., 2013, MNRAS, 429, 1425
Ruiz-Lapuente P., Lucy L. B., 1992, ApJ, 400, 127
Scalzo R., et al., 2014, MNRAS, 560
Scolnic D. M., Riess A. G., Foley R. J., Rest A., Rodney S. A., Brout D. J., Jones D. O., 2014, ApJ, 780, 37
Stritzinger M., Leibundgut B., Walch S., Contardo G., 2006, A&A, 450, 241
Stritzinger M. D., et al., 2011, AJ, 142, 156
Suntzeff N. B., 1996, ssr..conf, 41
Suntzeff, N. B. 2003, in: From Twilight to Highlight, The Physics of Supernovae, ed. W. Hillebrandt & B. Leibundgut, Heidelberg:Springer, 183
Tonry J. L., Dressler A., Blakeslee J. P., Ajhar E. A., Fletcher A. B., Luppino G. A., Metzger M. R., Moore C. B., 2001, ApJ, 546, 681
Tripp R., 1998, A&A, 331, 815
Truran J. W., Glasner A. S., Kim Y., 2012, JPhCS, 337, 012040
Wang B., Meng X.-C., Wang X.-F., Han Z.-W., 2008, ChJAA, 8, 71
Wang X., et al., 2008, ApJ, 675, 626
Wood-Vasey W. M., et al., 2008, ApJ, 689, 377
Zheng W., et al., 2014, ApJ, 783, LL24